The Reconsitution of the Weld Pool Surface in Stationary TIG Welding Process With Filler Wire

Jiankang Huang (sr2810@163.com)

State Key Laboratory of Advanced Processing and Recycling of Non-Ferrous Metals, Lanzhou University of Technology, Lanzhou 730050, China https://orcid.org/0000-0002-1257-8622

LIU Guangyin

Lanzhou University of Technology

HE Jing

Southern University of Science and Technology

YU Shurong

Lanzhou University of Technology

LIU Shien

Lanzhou University of Technology

CHEN Huizi

Lanzhou University of Technology

PAN Wei

Lanzhou University of Technology

FAN Ding

Lanzhou University of Technology

Original Article

Keywords: Weld pool surface, Specular reflection, TIG, Approximate algorithm, Filler wire

Posted Date: December 1st, 2020

DOI: https://doi.org/10.21203/rs.3.rs-116067/v1

The reconsitution of the weld pool surface in stationary TIG welding process with filler wire

HUANG Jiankang[1,*], LIU Guangyin[1], HE Jing[2,*], YU Shurong[3,*], LIU Shien[1], CHEN Huizi[1] , PAN Wei[1], FAN Ding[1]

1. State Key Laboratory of Advanced Processing and Recycling of Non-Ferrous Metals, Lanzhou University of Technology, Lanzhou 730050, China

2. Department of Mechanical Energy Engineering, Southern University of Science and Technology, Shenzhen 518055, China

3. Mechanical and Electrical College, Lanzhou University of Technology, Lanzhou 730050, China

Abstract: In order to study the dynamic characteristics of the weld pool surface during the TIG welding process of the filler wire, an observation test platform for the study of the three-dimensional surface behavior evolution of the TIG weld pool based on the grid structure laser was used to observe the weld pool surface and obtain the reflection grid laser image. The three-dimensional surface evolution of the fixed-point TIG welding pool is accurately restored by the three-dimensional recovery algorithm of the weld pool surface, so as to obtain the three-dimensional surface morphology of the weld pool. The difference between the obtained weld pool height and the experimental results is very small, and the results are basically the same.

Keywords: Weld pool surface; Specular reflection; TIG; Approximate algorithm; Filler wire

Nomenclature

a	Determined according to the actual size	k	Triangle similarity scale factor
B	Transformation matrix of 3*2	L	Endpoint line of grid transverse line
$H_{(i,j)}$	Distance from node $A_{(i,j)}$ to the endpoint connection L_j	O	Focal point of inverse ray
$h_{(i,j)}$	Weld pool height	O_{xyz}	Origin of laser source
I	Direction vector of incident light	*Greek symbols*	
I'	Directional vector of reflected light	α	*laser tilt angle*
		β	*correction factor*

1 Introduction

TIG welding has many advantages, such as high weld quality, ease of control the base metal heat input, and use of simple equipment, and thus it is widely used in industrial production[1]. Because of the limit of the tungsten electrode, the weld penetration of TIG welding is shallow, which can easily result in incomplete penetration[2]. Incomplete penetration in the welding process has a strong negative influence on the weld mechanical properties. Therefore, penetration is usually the focus of attention in the arc welding process[3].

The weld pool formed in welding contains a wealth of information that reveals the changing state, stability and penetration of the thermal process[4]. Observing the weld pool and obtaining its geometric information have become the key technologies in welding penetration control[5]. The ever-changing information of the relevant physical quantity in the welding process can be obtained effectively by sensing the information of the weld pool surface change[6]. For the welding process, this observation offers an effective method for monitoring the mechanical properties of weld, studying the complex

* Corresponding author:
HUANG Jiankang, Email: sr2810@163.com
HE Jing, Email: hejing0229@gmail.com
YU Shurong, Email: yushur1991@163.com
The study was financially supported by the National Natural Science Foundation of China (No. 51665034).

welding thermal physical process, and ensuring control of the weld penetration[7]. Scholars have used different methods to study weld pool geometry, e.g., weld pool oscillation detection[8], infrared sensing[9], radiographic sensing[10], and visual sensing[11], among others. These methods mostly extract one-dimensional or two-dimensional geometric information from the surface of the weld pool and, only one or a few of the features for welding penetration control[12]. In further work, the researchers found that the three-dimensional geometric information of the weld pool can better reveal the penetration situation of the weld. Current methods for three-dimensional geometric measurement offer stereo vision[13], shading recovery[14] and structured light[15]. Among these mothods, as a comparatively accurate method, structured light has attracted the attention of many researchers. The structured light method was first proposed by Zhang and Kovacevic[16]. The basic principle of the structured light method is, that with the use of reflection principle, the structured laser projects to the entire pool surface, and the reflection of the laser irradiates a screen. The images on the screen are captured by a CCD industrial camera, to collect images of the structured laser with the weld pool shape changes and extract the spatial geometric relationship between the projection point and the reflection point. According to selected mathematical computations, the surface morphology of the weld pool can be recovered. To obtain a better improvement in accuracy, Wang et al.[17] ameliorated structured light and collected better clear images under strong arc light. Liu et al.[18]proposed a phase change correction method based on a linear ratio for measurement of the surface depth of the TIG weld pool, and obtained satisfactory results. Wang[19] proposed a new system based on the structured light method that satisfactiorily measured the 3-D weld pool shapes. Our research group also performed certain preliminary studies on the structured light method[20]. The result shows that a certain relationship exists between the penetration of the weld and the concavity and convexity of the weld pool surface. Via the surface of the weld pool, the dynamic welding process and surface concavity or convexity can be studied. Therefore, the weld penetration state can be controlled according to the geometrical parameters and shape of the weld pool surface. This experimental design hardly recovers the geometrical parameters and shape of the weld pool surface accurately. Based on this observation, the experimental design is modified, and a new approximate mathematical algorithm is proposed to accuratdly obtain the geometrical parameters and shape of the weld pool surface.

Thus far, most research on the weld pool surface in TIG welding via the structured light method has not covered the addition of filler wire. Use of filler wire is common in TIG welding for industrial applications. The aim of this paper is to better study the dynamic behavior of the weld pool surface in TIG welding with filler wire. In this paper, a modified measurement system and the new proposed approximate algorithm were to observe and analyze the surface changes in stationary TIG welding with filler wire. The validity and accuracy of the new method were tested.

2 The fast algorithm of reconstruction

The measurement system with a grid laser is shown in Fig. 1. This system is established based on the light reflection law. The smooth weld pool surface conforms to the specular reflection, whereas the rough workpiece surface conforms to diffuse reflection. Based on the light reflection law, and the difference between the weld pool and the base material in diffuse reflection, the grid laser is projected onto the surface of the weld pool and reflected from the surface of the weld pool. The reflection is intercepted by a screen. The changing process of the laser grid on the screen is captured by a camera, and the images on the screen are analyzed and recorded. The three-dimensional weld pool surface can be recovered via an approximate algorithm.

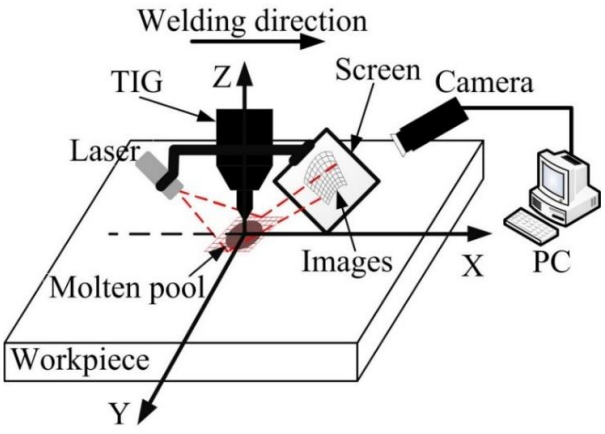

Fig. 1. Experimental diagram of measurement using grid laser vision.

The following illustration of Fig. 2 presents the schematic diagram and parameter settings of the weld pool surface recovery process:

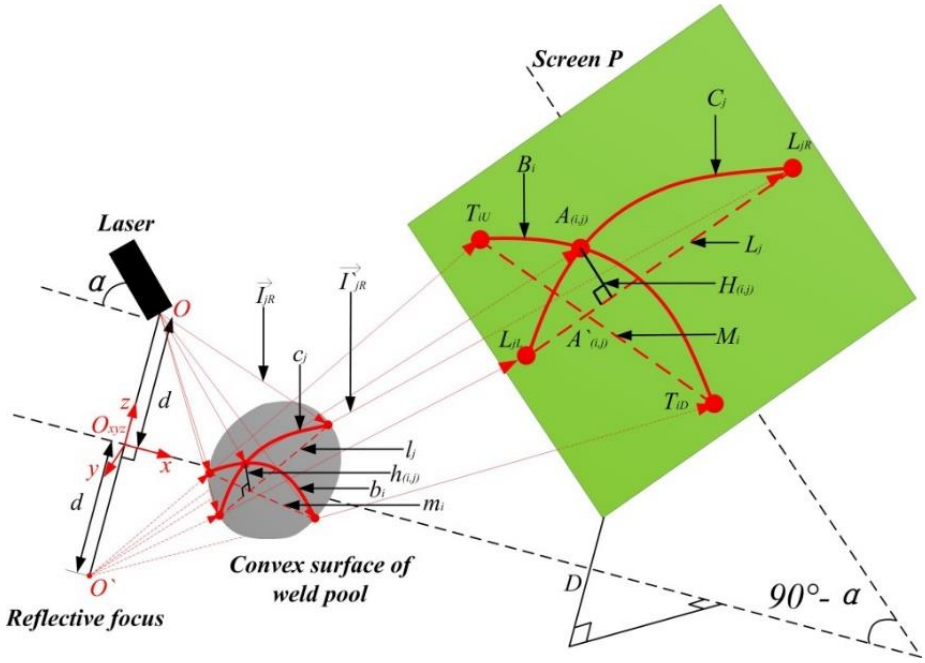

Fig. 2. Diagram of the reflection of the weld pool and calibration of its parameters.

A new algorithm for surface restoration of the weld pool is established, and its calculation flow is shown in the following Fig. 3:

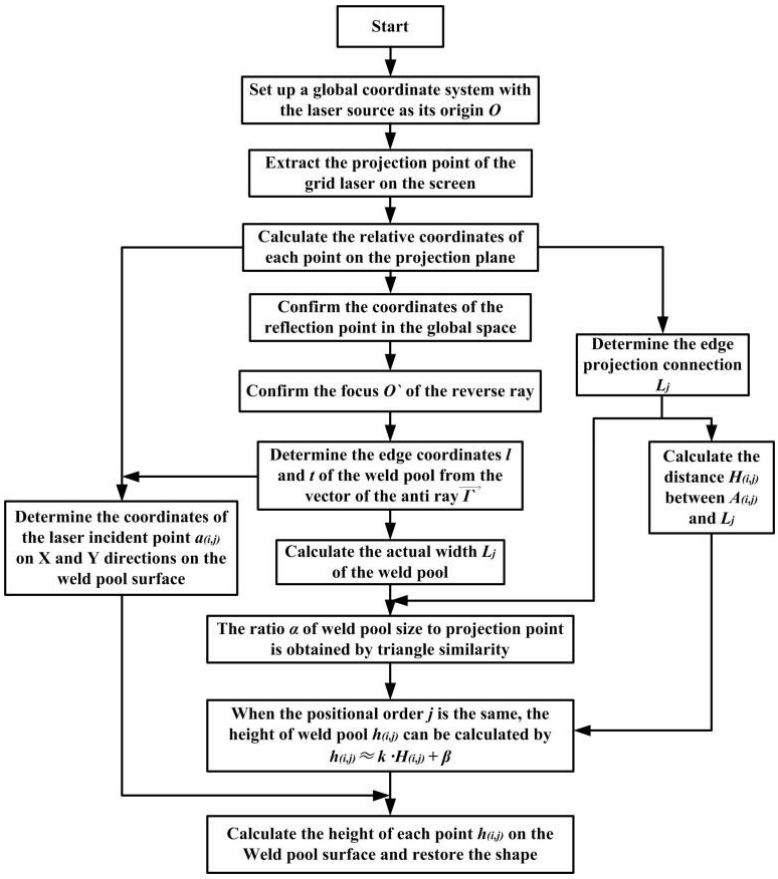

Fig. 3. Flow chart of the algorithm.

In the process of recovering the weld pool surface, the following simplifications were applied:

As shown in Fig. 4, the grid laser projects onto the surface of weld pool, and the reflection of the *XZ* section

is shown in the diagram. The location of the reflection point in the center of the weld pool is different from that at the edge of the weld pool in the *X* direction, which is affected by the height of the weld pool. Because the pool height is noably small, this difference can be ignored.

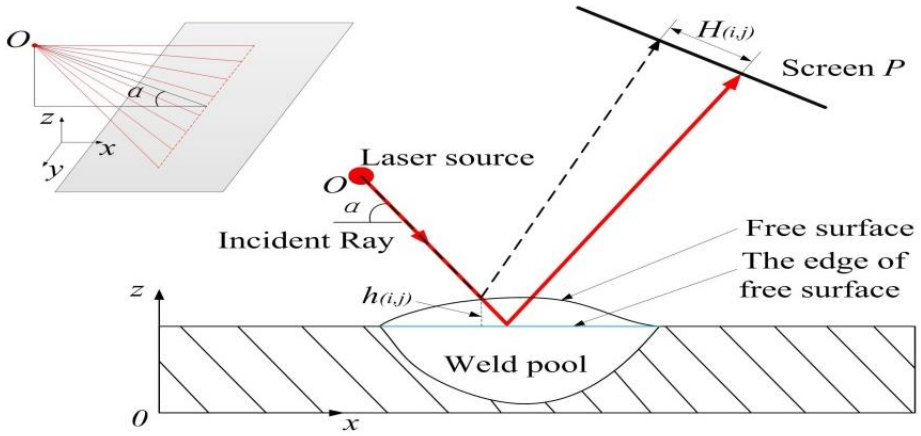

Fig. 4. Reflection diagram of the *XZ* section.

The pool height $h_{(i,j)}$ has a corresponding proportional relationship with the distance $H_{(i,j)}$ from the projection point $A_{(i,j)}$ to its corresponding auxiliary line L_i. From Fig. 5, the following relationship based on triangle similarity is obtained：

$$\frac{O'C_1}{O'C}=\frac{T_UT_D}{T_{OU}T_{OD}}=a \tag{1}$$

In addition, the a is determined according to the actual size.

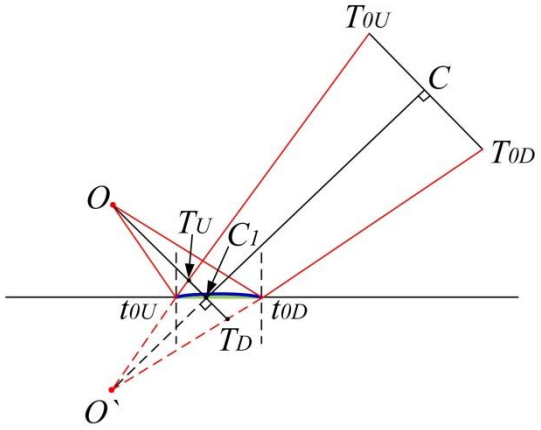

Fig. 5. Proportional relationship of the reflection model.

The specific method of calculation is given as follows: after setting the projection point, which is obtained from the orthographic projection of the laser source to the plane of the weld pool surface, as the origin $O_{xyz}(0, 0, 0)$, the three-dimensional Cartesian coordinate system is established. The coordinate of the grid laser source in the space is $O(0, 0, z_0)$ and the incident light projected onto the weld pool surface is described by:

$$\frac{x-x_0}{I_x}=\frac{y-y_0}{I_y}=\frac{z-z_0}{I_z}=t' \tag{2}$$

where $I=(I_x,I_y,I_z)$ is the direction vector of the incident light, and based on Fig. 2, z_0 is the height d of the laser source.

The boundary of the weld pool contains abundant geometric information. The weld pool height is approximately *0*, and the laser obeys the principle of specular reflection. The reflected long line of the laser projecting to the boundary of the weld pool is assigned given a point in the space, which can be treated as the focal point of the reflected ray. It is symmetrical to the plane of the laser source on the weld pool, and the focal point of the inverse ray is $O'(0, 0, -z_0)$.

Thus, the reflected rayslaser counter rays at the boundary can be obtained as follows:

$$\frac{x-x_0}{I_x}=\frac{y-y_0}{I_y}=\frac{z-z_0}{I_z}=t \tag{3}$$

where $I'=(I_x^{'},I_y^{'},I_z^{'})$ is the directional vector of the reflected light of the boundary.

The appearance of the grid laser on the screen P is enhanced at the node and the endpoint. The highlight node in the center of the laser projection is the origin $A_{(0,0)}$ of the screen plane. Base on this arrangement, the grid line and intersection point of the laser are calibrated according to the corresponding position. The longitudinal lines on the screen P are B_i, and the transverse lines are C_i. The endpoint is calibrated according to the location of the grid line, as shown in Fig. 6.

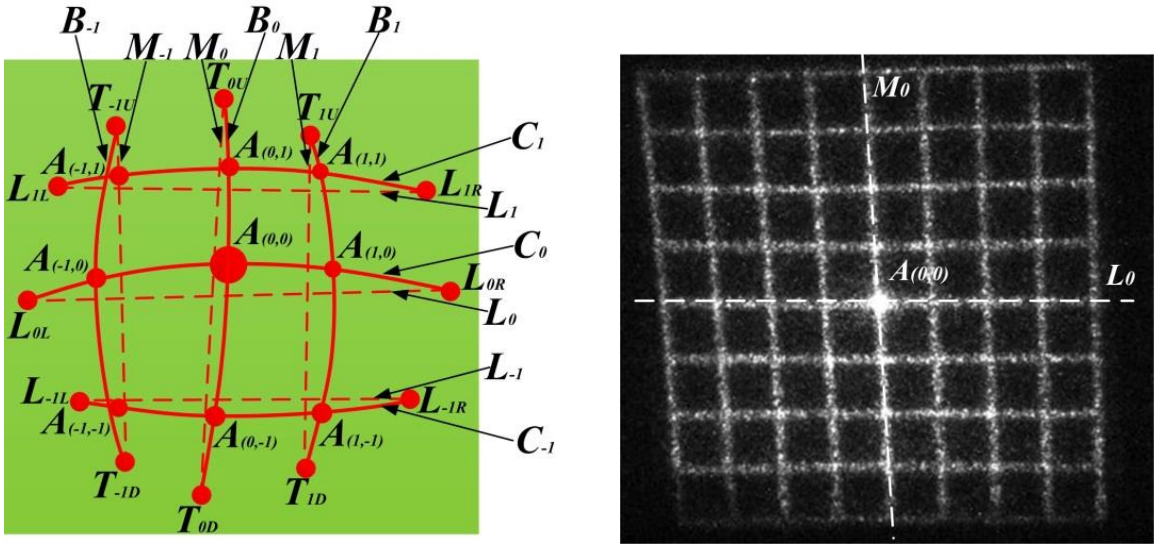

Fig. 6. Calibration of the grid laser on the screen.

The coordinates of the endpoints of the grid on the screen plane are obtained through the transpose matrix B, and the coordinates are expressed as follows:

$$L^{'} = BL = B\begin{bmatrix} x_{i,j} \\ y_{i,j} \end{bmatrix} = \begin{bmatrix} x^{'}_{i,j} \\ y^{'}_{i,j} \\ z^{'}_{i,j} \end{bmatrix} \tag{4}$$

where B is a matrix of 3*2, and its specific parameters are determined by the location of $A_{(0,0)}$ in the global coordinates of the space.

The direction vector I` of the reflected light of the weld pool can be obtained by combining the focal coordinates and the coordinates of the points on the screen. The specific parameters of the laser reflection line at the weld pool boundary can be obtained. The intersection of the laser reflection line and the plane $z=0$ is the boundary of the weld pool, and the coordinates of the laser projected on the edge of the weld pool can be determined.

According to the first assumption, when the laser tilt angle α is large, the grid transverse line c_i of the grid laser projecting to the weld pool surface is approximately the same in the X direction, i.e., the endpoint line l_j of the grid transverse line has the same coordinates in the X direction.

The plane, formed by the grid transverse line M_i and the focus O' of the reflected laser, intersects with the surface of the weld pool, and the intersection line b_i can be obtain. The end points of the intersection b_i at the edge of the weld pool are t_{iU} and t_{iD}, and the endpoint connection m_i can be approximated as the projection of the radiation b_i on the plane $z=0$. Therefore, the intersection point between the connection l_j and the connection M_i is the projection of the grid laser node $a_{(i,j)}$ on the plane $z=0$, and they have the same coordinates in the directions of X and Y.

On the screen P, the distance from node $A_{(i,j)}$ to the endpoint connection L_j is $H_{(i,j)}$, which is proportional to the height of $a_{(i,j)}$ at the corresponding node of the weld pool surface.

Because the reflection of the grid laser on the surface of the weld pool presents specular-like reflection, the height of the projecting point in the pool affects its position on the screen P, and the triangle similarity can prove the relationship.

The distance from the projection point $A_{(i,j)}$ to its corresponding auxiliary line L_j is $H_{(i,j)}$, the reflection point of the weld pool surface corresponding to $A_{(i,j)}$ is $a_{(i,j)}$, and the height of the weld pool is $h_{(i,j)}$.

According to the first assumption, when the incidence angle α is larger, the following relationship exists：

$$h_{(i,j)} \approx kH_{(i,j)} + \beta \tag{5}$$

By combining the coordinates of $a_{(i,\ j)}$ in X and Y directions obtained in Formula 3, the coordinates of each reflection point $a_{(i,j)}$ in the global space can be determined.

According to the reconstruction principle of the three-dimensional surface of the weld pool, the known surfaces can be recovered to verify the accuracy and feasibility of the algorithm via a program. The laser beam is projected onto a known Gaussian surface, which has reflective properties. A screen with an angle of 45° to the X axis is placed on the path of the laser reflection line, and the reflected laser is projected onto the screen, as shown in Fig. 7. The data of the projected image on the screen can be measured and extracted, and the recovered surface can be calculated. Finally, by comparing the

restored Gaussian surface with the known surface, we can obtain the error between them.

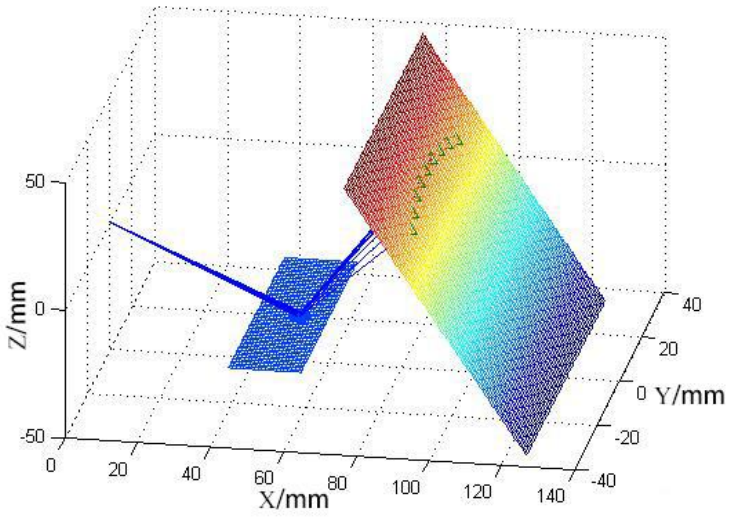

Fig. 7. Calibration of the grid laser on the screen.

The recovery processes of the Gaussian convex and concave surfaces, are shown in Fig. 8 and Fig. 9, respectively, where Fig. 8(a) is the position of the standard Gaussian convex surface in space. Fig.8(b) is the imaging of the laser beam reflected on the screen, and Fig.8(c) is a convex surface restored by the calculation.

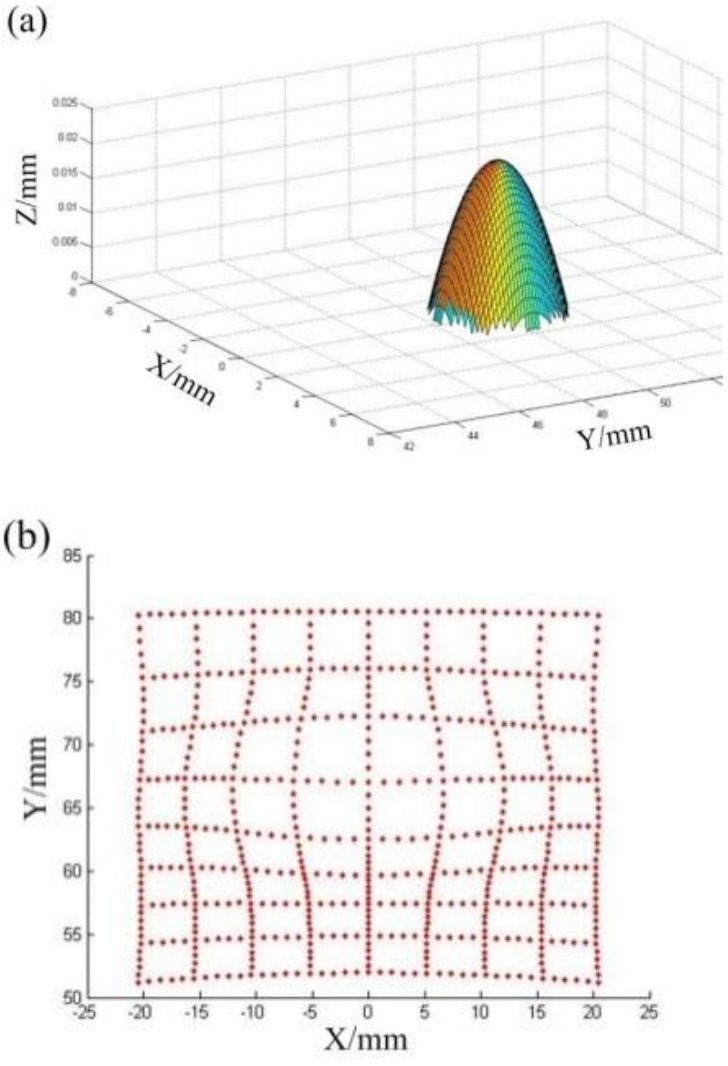

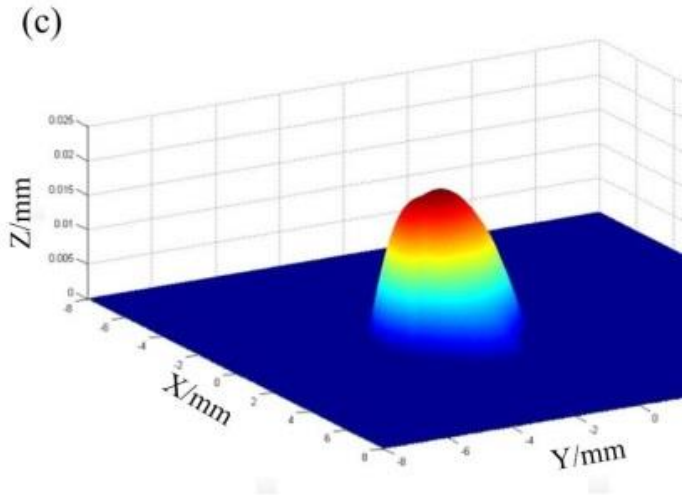

Fig. 8. Recovery process of Gaussian convexity: (a) standard Gaussian convexity (b) projection of the grid laser on the screen, (c) recovered surface.

The Gaussian concave surface is verified and restored in a similar manner. The main steps are the same as described above. Fig. 9(a) is the position of the standard Gaussian concave surface in space. Fig.9 (b) is the imaging of the laser beam reflected on the screen, and Fig. 9 (c) is a concave surface restored by the calculation.

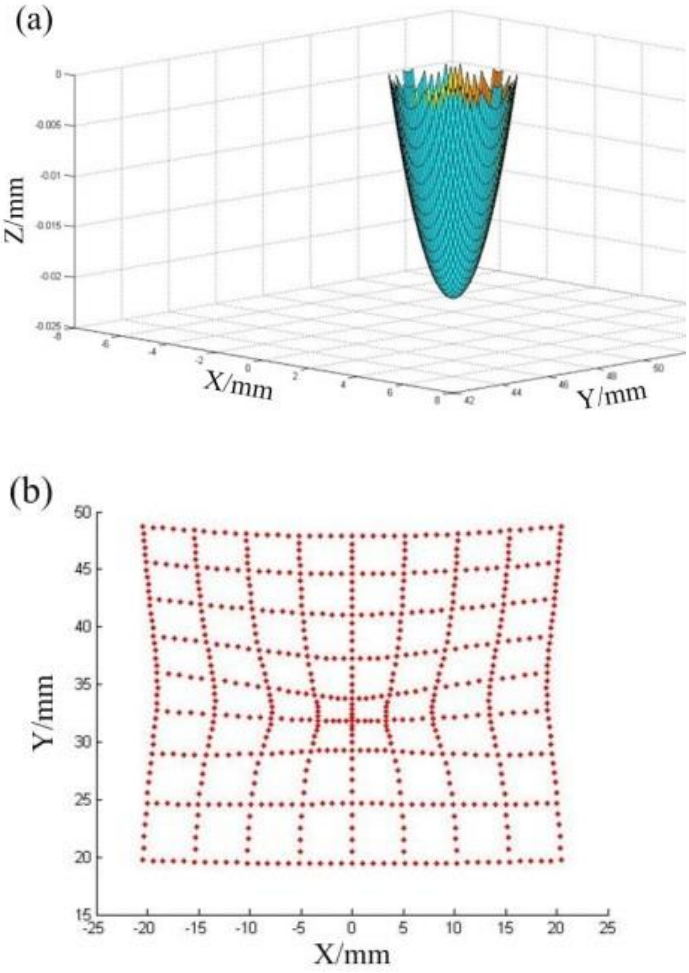

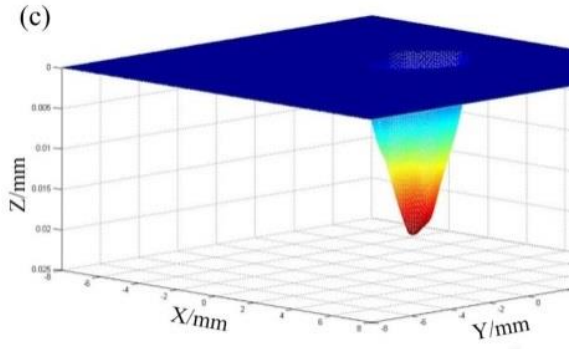

Fig. 9. The recovery process of Gaussian concavity: (a) standard Gaussian concavity (b) the projection of grid laser on the screen (c) the recovered surface.

Table 1 shows the verification results of the Gaussian surface and their comparison with standard the surface. It can be observed from the results that the algorithm has a better effect on the recovery of convexity and concavity. The calculated results show good conformation to the actual value.

Table 1 Verification results and accuracy comparison.

		Standard surface	Recovery surface
Gaussian convexity	Height/mm	0.022097	0.021609
	Radius/mm	2	1.965
Gaussian concavity	Height/mm	0.022097	0.024493
	Radius/mm	2	1.89

3 Reconstruction of the weld pool surface

Fig.10 is a schematic diagram of TIG welding droplet transition, which describes the process of welding wire being heated by the arc to melt into droplets and enter the weld pool, and the process of weld pool surface changes after the droplets enter the weld pool.

The surface of the weld pool can reflect the welding quality. To obtain high level of welding quality, we analyze the dynamic behavior of the pool surface in stationary TIG welding with filler metal. The most important and direct external performance aspect of TIG welding with filler wire is the impact action of the droplet on the weld pool. The droplet impact on the weld pool is a complex and multi-factorial process. Many types of forces act on droplets, including pressure, surface tension, and gravity. At the same time, the droplet transfers to the weld pool with high speed in the transient process, and a high speed camera is necessary to capture the real-time droplet transfer information.

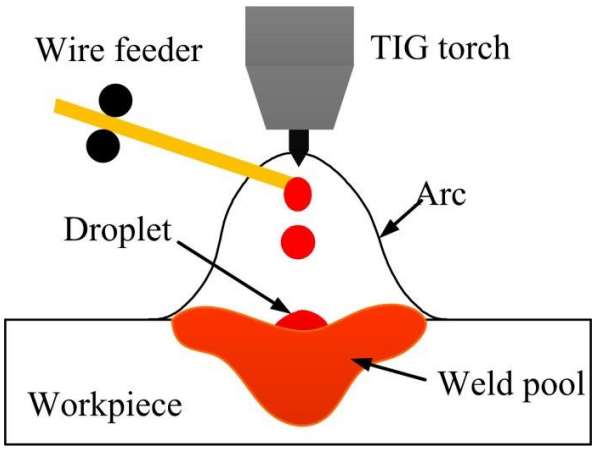

Fig. 10. Diagram of the drop transfer model for TIG welding.

Based on the above experimental system, the reconstruction of weld pool surface in stationary TIG welding is studied. The grid laser is customized according to the test requirements, as shown in Fig. 11. The camer is a MV-GED30M CCD industrial camera, and 304 stainless steel with 125 × 50 × 30 mm^3 dimensions is used in the workpiece. The welding current is 40A, the flow rate of argon gas is 10 L/min, the diameter of the welding wire is 0.8 mm, and the size of experimental system is measured as d=11.32 mm and D=59.40 mm. In this experiment, only one droplet is studied. During stationary TIG welding, the welding wire is inserted by hand. After one drop falls, the welding wire is pulled out. The wire feed angle and the distance to the specimen are approximately 45° and ~2.5 mm, respectively.

The entire welding process was detected by the above experimental observation system. The three-dimensional information of the weld pool surface was obtained by analysis and measurement, and the weld pool surface is reconstructed in three dimensions.

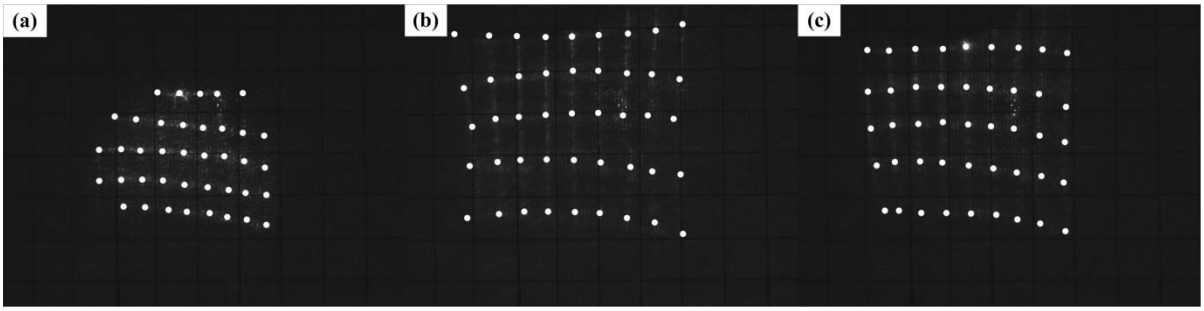

Fig. 11. Imaging of the grid laser: (a) T=0s (b) T=0.05s, and (c) T=0.13s.

Fig. 12 shows the real-time reconstruction result of the three dimensional surface according to the reflection imaging of the grid laser. Fig. 12(a) presents the three-dimensional restoration of the weld pool surface when the welding wire is unfilled, which is a typical convex surface. Fig. 12(b) displays the morphology of the three-dimensional surface after the droplet enters the weld pool approximately 0.05 s. It can be observed that the center of the weld pool is severely deformed by the droplet impact. The center of the weld pool is depressed, the free surface height of the weld pool increases by approximately 0.0127 mm compared with that when the droplet enters, and the width of the weld pool increases about by approximately 0.09 mm. Fig. 12(c) shows the morphology of the three-dimensional surface after the droplet enters the weld pool approximately 0.13 s. Compared with the observation at 0.05 s, the surface center of the weld pool is restored to a convex shape, and the surface height and the width of the weld pool change minimally. The measured results are shown in Fig.13.

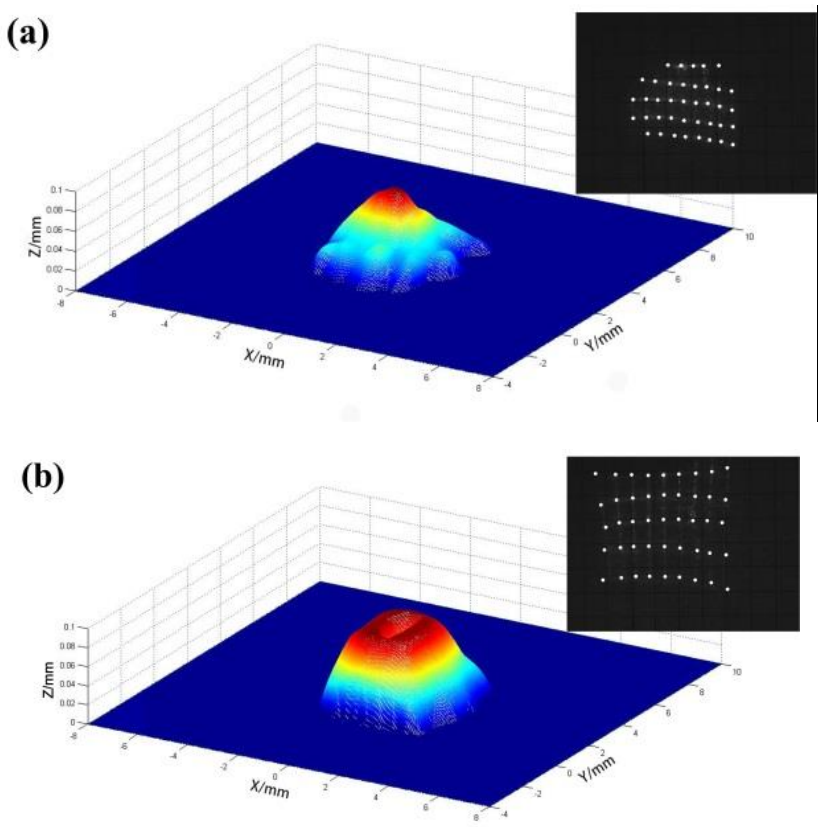

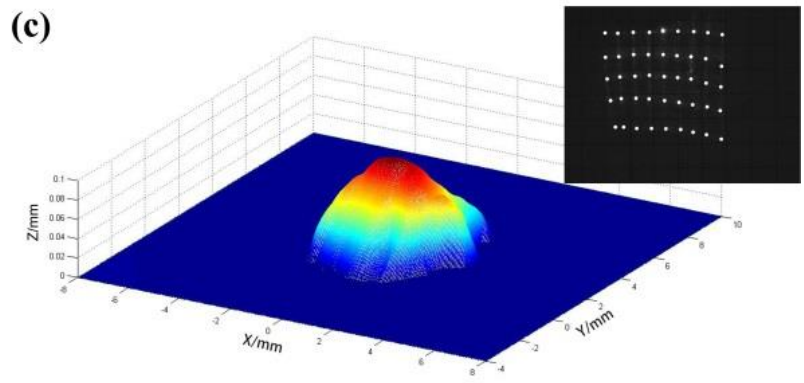

Fig. 12. Reconstruction of the droplet dropping process: (a)T=0 s, (b)T=0.05 s, (c)T=0.13 s.

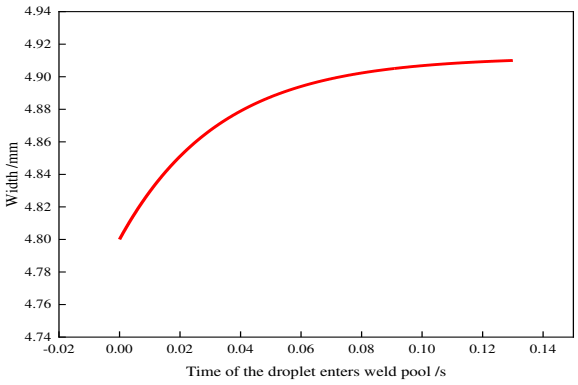

(a) The width of weld pool

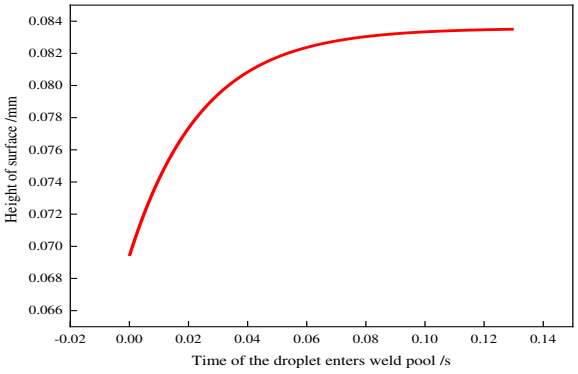

(b) Height of surface

Fig. 13. Comparison of experimental results and recovery results.

Fig. 14 presents the cross-sectional comparison between the test results and the recovery results. Certain errors occur between the two results, and the recovery result is smaller than the test result, which is consistent with the verification results.

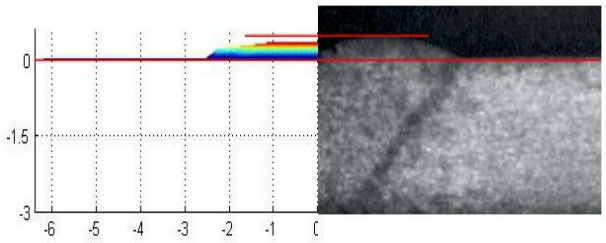

Fig. 14. Cross section comparison between test results and recovery results.

4 Conclusion

To study the dynamic weld pool surface in TIG welding with filler wire, an algorithm based on the mirror reflection principle is used to recover the free surface of the weld pool when the droplet falls into it. The following conclusions can be obtained in this work:

(1) Through the TIG welding pool three-dimensional surface behavior evolution test platform, we collected the information about the change of the three-dimensional surface of the weld pool when the droplet entered the weld pool.

(2) Through three-dimensional recovery, it is observed that when the droplet enters the weld pool for 0.05 seconds, the center of the weld pool is sunken. When the droplet enters the weld pool for 0.13 seconds, the weld pool returns to a convex shape and the free surface rises by 0.0141mm, and the width increases by 0.11mm .

(3) The recovery results of the weld pool surface show that this algorithm can effectively reflect the change of concavity and convexity of the weld pool surface. A small error occurs between the experimental results and the

recovery results of the weld pool morphology, and the overall morphology is consistent, which proves that the recovery method is feasible.

Declaration

Ethics approval and consent to participate

The manuscript is ethically approved and all authors agree to participate.

Publication

The authors all agree to publish.

Availability of data and materials

All authors promise that materials and data are authentic.

Authors' Contributions

HUANG Jiankang and FAN Ding propose the research project, and conceived and designed the study and revised the manuscript; LIU Guangyin study the welding process and wrote the manuscript; HE Jing and YU Shurong improve the research by theory and revised the manuscript; LIU Shien, CHEN Huizi and PAN Wei assisted in numerical analysis and experimental verification. All authors read and approved the final manuscript.

Competing Interests

The authors declare no competing financial interests.

Biographical notes

HUANG Jiankang, is currently an associate professor in Lanzhou University of Technology, China. His research interests include numerical simulation of welding and arc additive manufacturing.

E-mail:sr2810@163.com

LIU Guangyin, is a currently master degree candidate in Lanzhou University of Technology, China. His research interests include numerical simulation.

E-mail: 15023860381@163.com

HE Jing, is a faculty in Southern University of Science and Technology, China. His research interests include welding process and additive manufacturing.

E-mail: hejing0229@gmail.com

YU Shurong, is currently a professor in Lanzhou University of Technology, China. His research interests include arc additive manufacturing.

E-mail: yushur1991@163.com.

LIU Shien, is a currently student in Lanzhou University of Technology, China. His research interests include dissimilar metal connection and arc additive manufacturing.

E-mail: 18894007605@163.com

CHEN Huizi, is a currently student in Lanzhou University of Technology, China. His research interests include dissimilar metal connection and arc additive manufacturing.

E-mail: huizi943121418@163.com

PAN Wei, is a currently master degree candidate in Lanzhou University of Technology, China. His research interests include additive manufacturing.

E-mail: pyw910108@163.com

FAN Ding, is currently a professor in Lanzhou University of Technology, China. His research interests include numerical simulation of welding and arc additive manufacturing.

E-mail: fand@lut.cn;

Acknowledgements

We are grateful for the technical and financial support provided by Lanzhou University of Technology, National Natural Science Foundation of China.

Funding

This work was funded by National Natural Science Foundation of China (No.51665034).

References

[1] K.H. Tseng, C.Y. Hsu, Performance of activated tig process in austenitic stainless steel welds, Journal of Materials Processing Technology, 211(2011) 503-512.

[2] P.J. Modenesi, E.R. Apolinário, I.M. Pereira, TIG welding with single-component fluxes, Journal of materials processing technology, 99(2000) 260-265.

[3] J.J. Wang, T. Lin, S.B. Chen, Obtaining weld pool vision information during aluminium alloy TIG welding, The International Journal of Advanced Manufacturing Technology, 26(2005) 219-227.

[4] P.C. Zhao, C.S. Wu, Y.M. Zhang, Numerical simulation of the dynamic characteristics of weld pool geometry with step-changes of welding parameters, Modelling & Simulation in Materials ence & Engineering, 12(2004) 765.

[5] C.S. Wu, J. Chen, Y.M. Zhang, Numerical analysis of both front- and back-side deformation of fully-penetrated gtaw weld pool surfaces, Computational Matericals ence, 39(2007) 0-642.

[6] G. Saeed, Y.M. Zhang, Mathematical formulation and simulation of specular reflection based measurement system for gas tungsten arc weld pool surface, Meas. Sci. Technol, Measurement ence & Technology 14(2003) 1671.

[7] H. Fan, N.K. Ravala, H.C.W. Iii, B.A. Chin, Low-cost infrared sensing system for monitoring the welding process in the presence of plate inclination angle, Journal of Materials Processing Technology, 140(2003) 668-675.

[8] A. Liu, X. Tang, F. Lu, Weld pool profile characteristics of al alloy in double-pulsed GMAW, The International Journal of Advanced Manufacturing Technology, 68(2013) 2015-2023.

[9] H.C.W. Iii, S. Kottilingam, R.H. Zee, B.A. Chin, Infrared sensing techniques for penetration depth control of the submerged arc welding process, Journal of Materials Processing Technology, 113(2001) 228-233.

[10] A.C. Guu, S.I. Rokhlin, Arc weld process control using radiographic sensing, Mater. Eval, 50(1992) 1344-1348.
[11] Z.M. Liu, C.S. Wu, J.Q. Gao, Vision-based observation of keyhole geometry in plasma arc welding, International Journal of Therm ences, 63(2013) 38-45.
[12] Z.J. Wang, G.J. Zhang, Z.M. Liang, Y.M. Zhang, H.M. Gao, L. Wu, Current status and development trend of tridimensional monitoring and measurement technology for weld pool surface, Welding Journal, 8(2007) 15-19.
[13] M. Dinham,G. Fang, Autonomous weld seam identification and localisation using eye-in-hand stereo vision for robotic arc welding, Robotics and Computer-Integrated Manufacturing, Robot. Cim.-Int. Manuf, 29 (2013) 288-301.
[14] L.P. Li, T. Lin, S.B. Chen, X.Q. Yang, The surface height acquisition of welding pool based on shape from Shading(SFS), Journal of Shanghai Jiaotong University, 40(2006) 97-107.
[15] L. Huang, C.S. Ng, A.K. Asundi, Dynamic three-dimensional sensing for specular surface with monoscopic fringe reflectometry, Optics Express, 19(2011) 12809-12814.
[16] Y.M. Zhang, R. Kovacevic, Real-time sensing of Sag geometry during GTA welding, Journal of Manufacturing ence & Engineering, 119(1997) 151-160.
[17] Z.Z. Wang, Y.M. Zhang, R.G. Yang, Analytical reconstruction of three-dimensional weld pool surface in GTAW, Journal of Manufacturing Processes, 15(2013) 34-40.
[18] Y.Q. Wei, N.S. Liu, X. Hu, X.P. Ai, Phase-correction algorithm of deformed grating images in the depth measurement of weld pool surface in gas tungsten arc welding, Optical. Engineering, 50(2011) 057209.
[19] Z.Z. Wang, An imaging and measurement system for robust reconstruction of weld pool during arc welding, IEEE Transactions on Industrial Electronics, 62(2015) 5109-5118.
[20] J.K. Huang, J. He, X.Y. He, S.R. Yu, D. Fan, Study on dynamic development of three-dimensional weld pool surface in stationary GTAW, High Temperature Materials and Processes, 37(2017) 455-462.

Figures

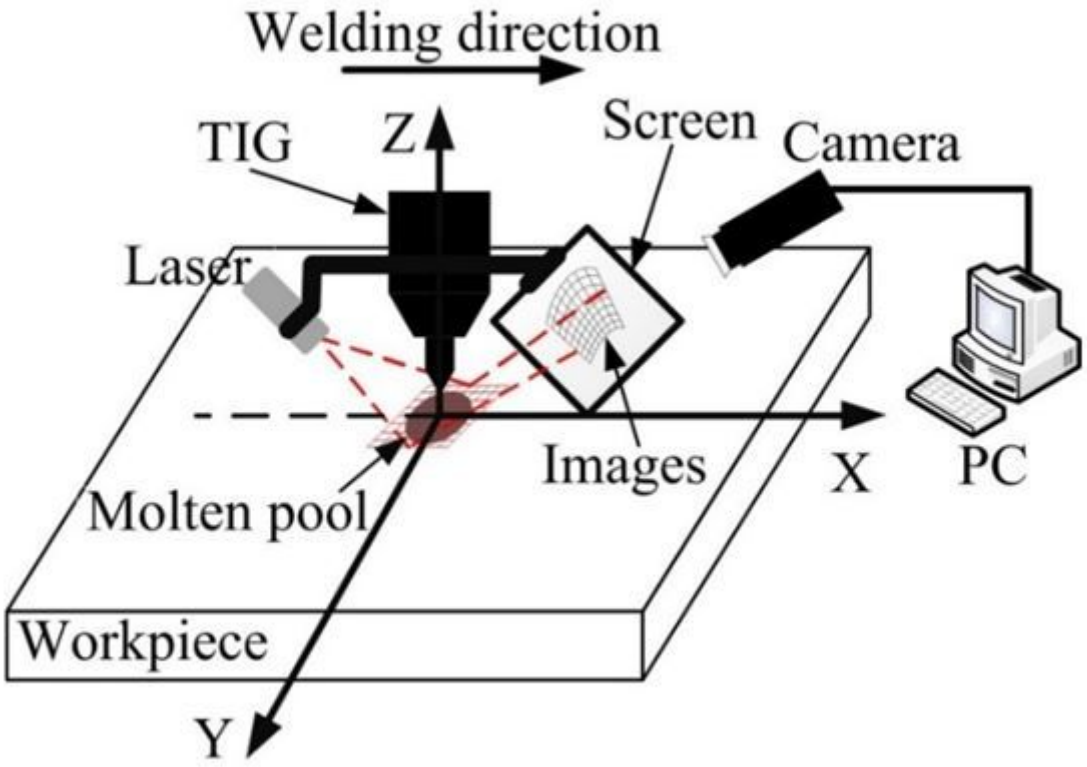

Figure 1

Experimental diagram of measurement using grid laser vision

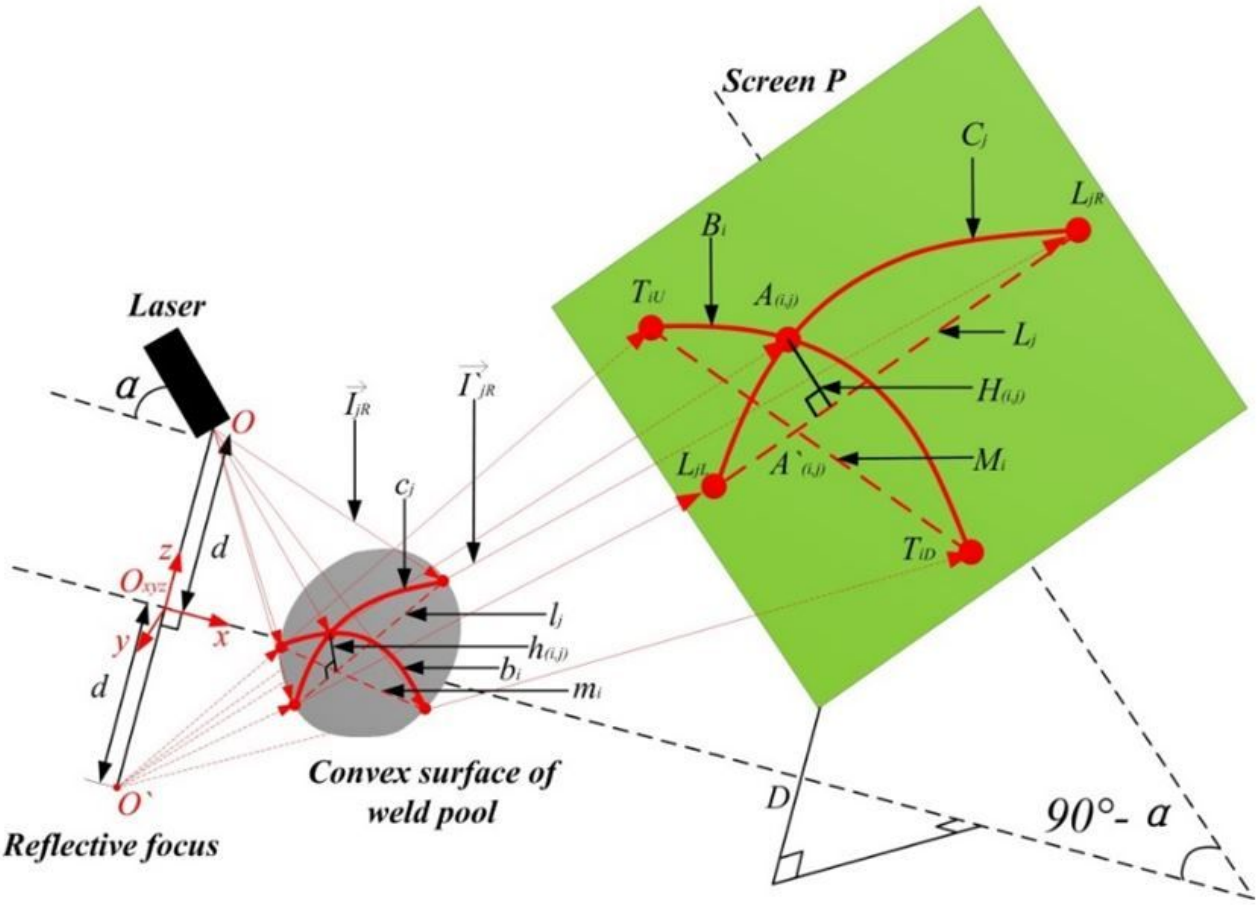

Figure 2

Diagram of the reflection of the weld pool and calibration of its parameters

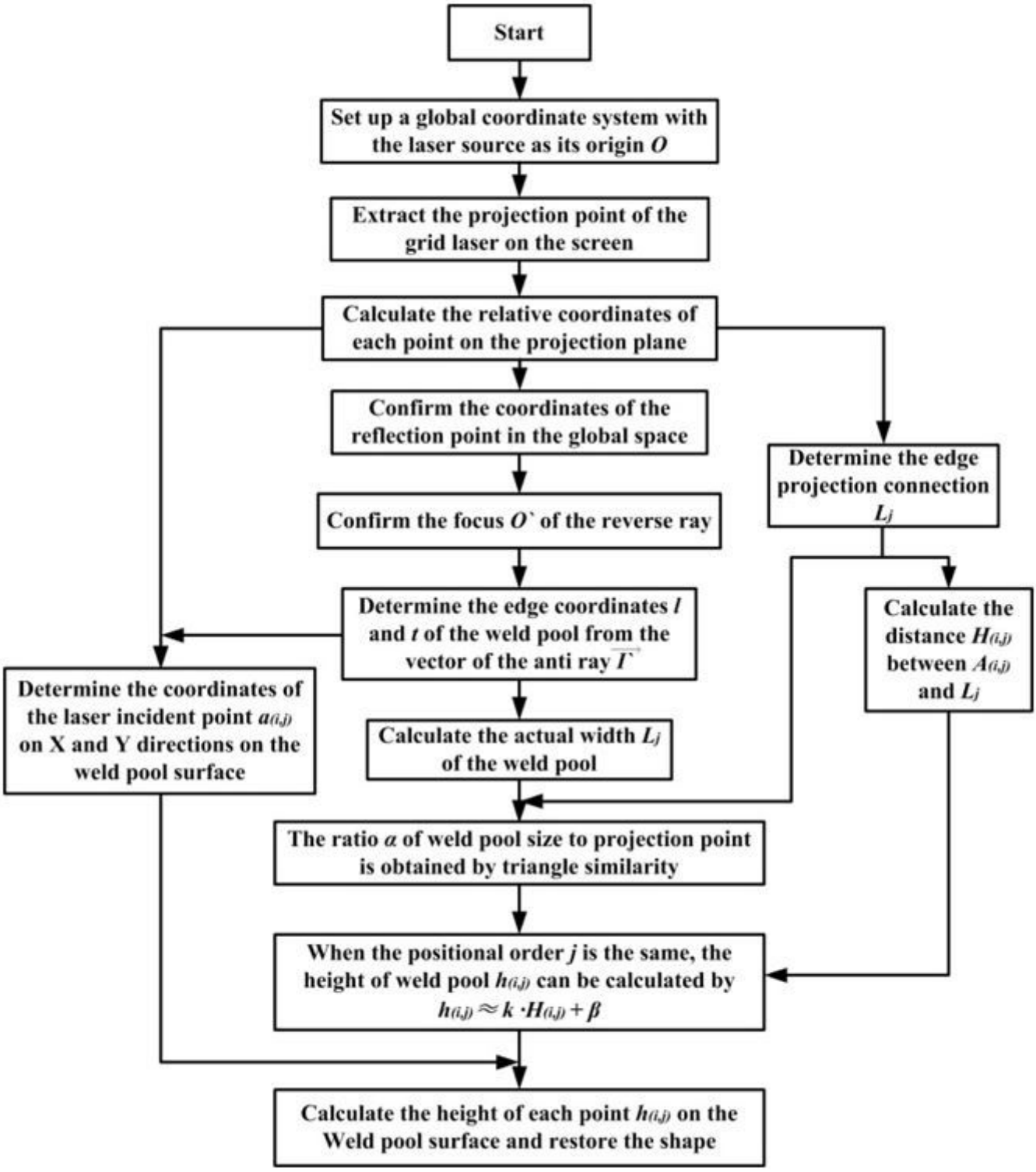

Figure 3

Flow chart of the algorithm

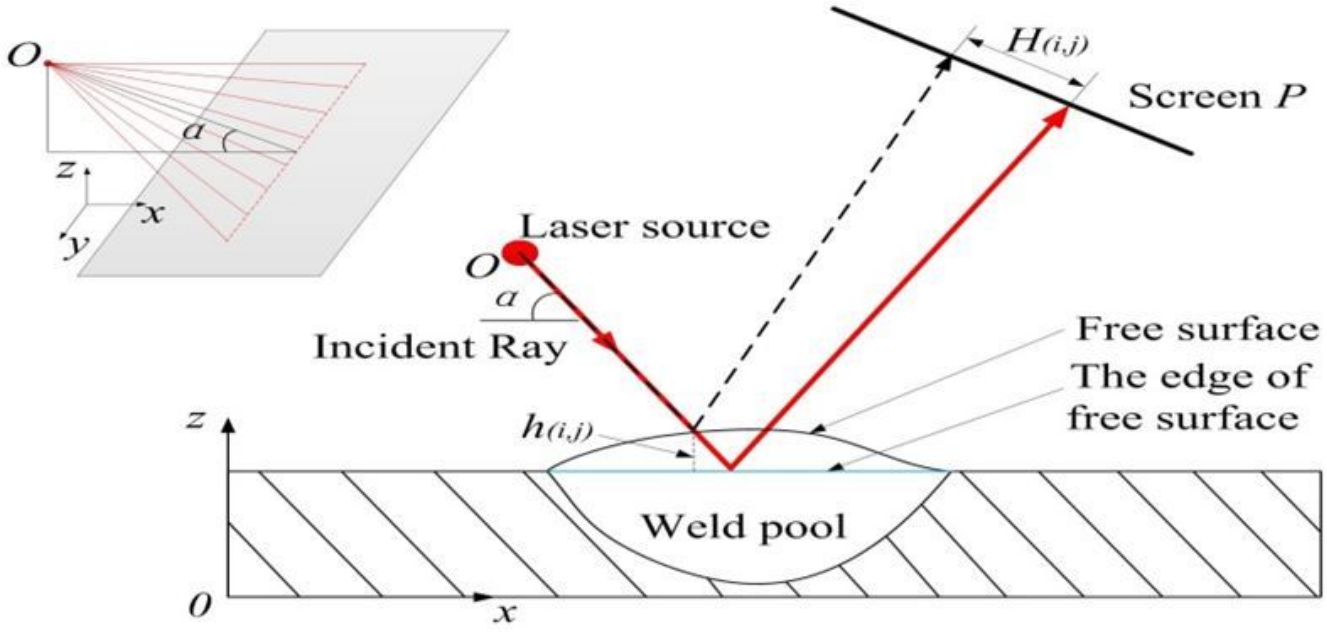

Figure 4

Reflection diagram of the XZ section.

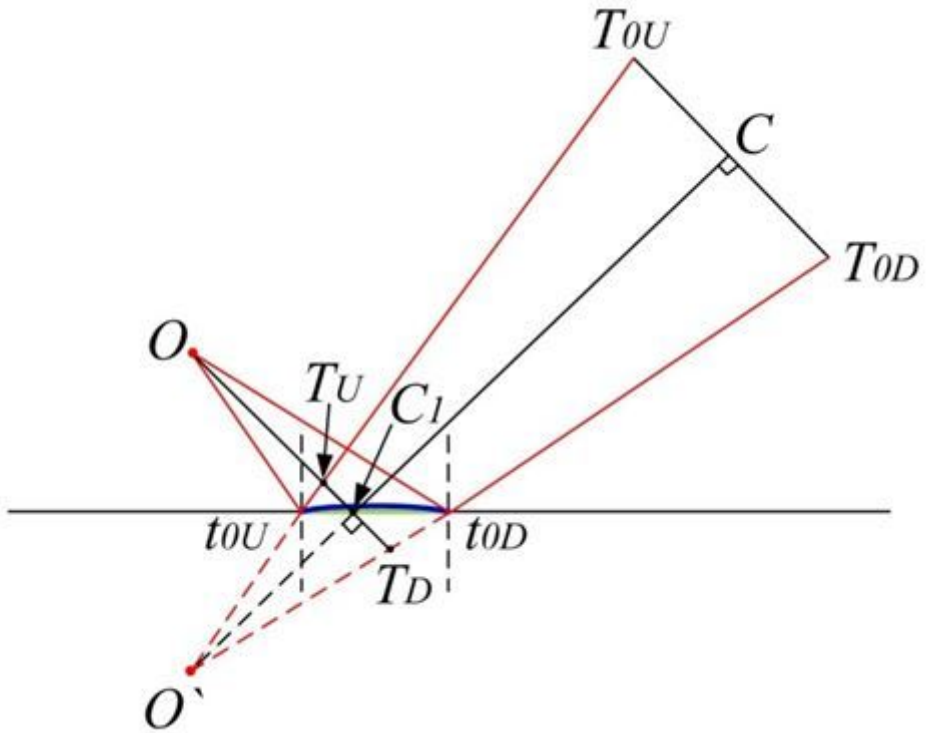

Figure 5

Proportional relationship of the reflection model.

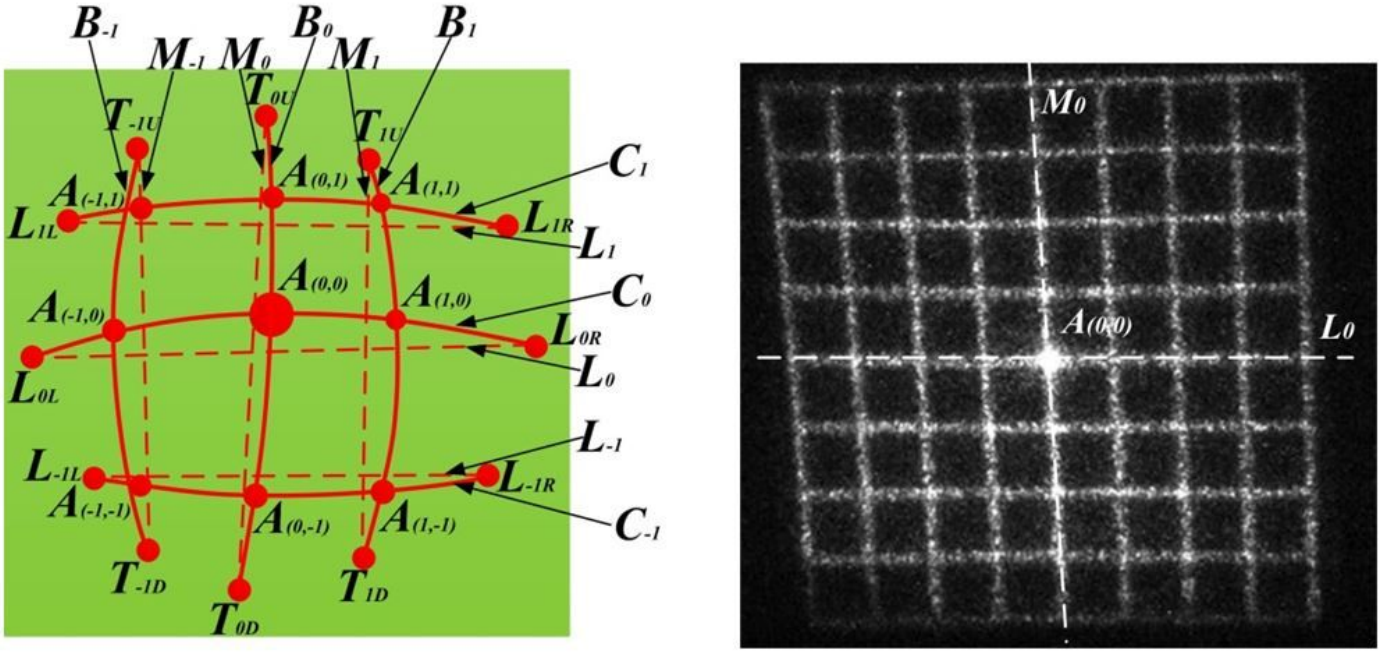

Figure 6

Calibration of the grid laser on the screen.

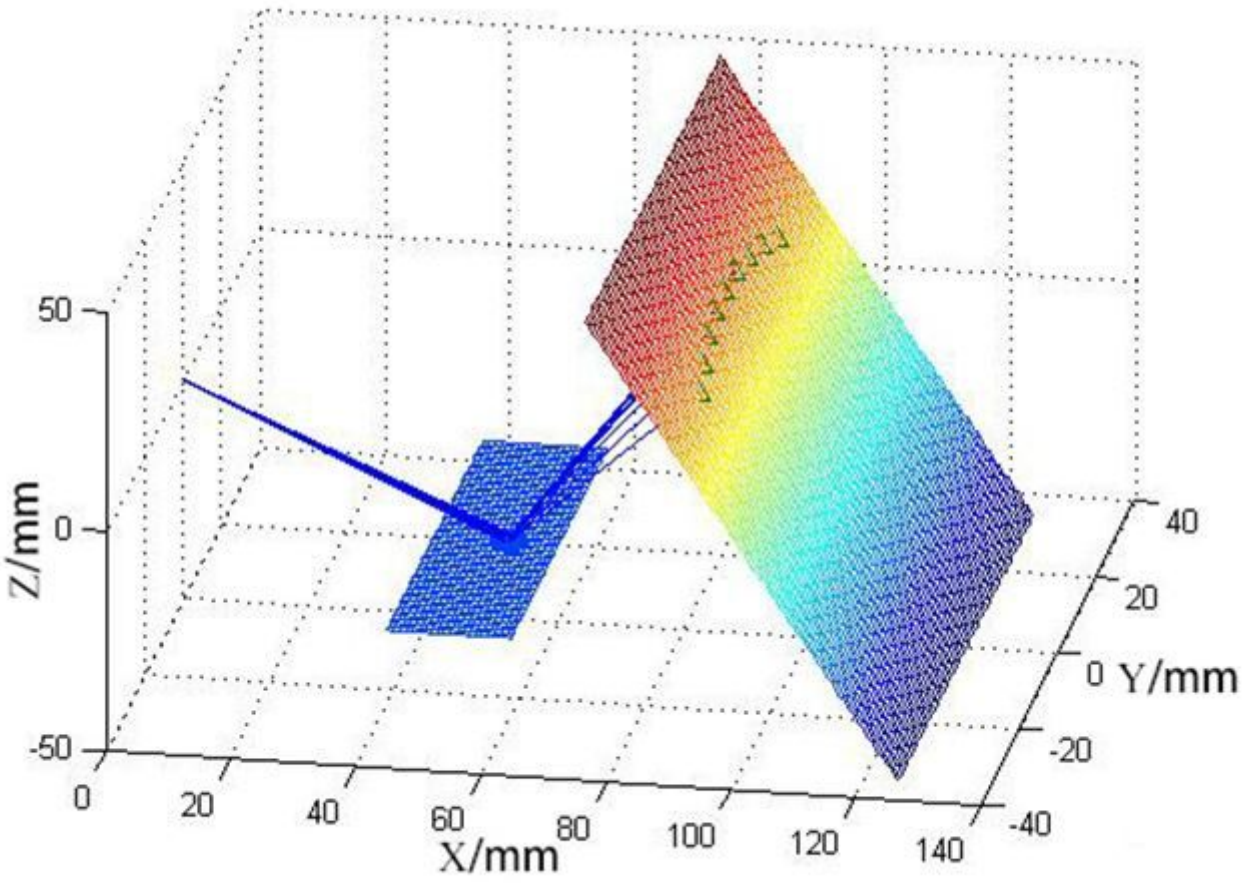

Figure 7

Calibration of the grid laser on the screen

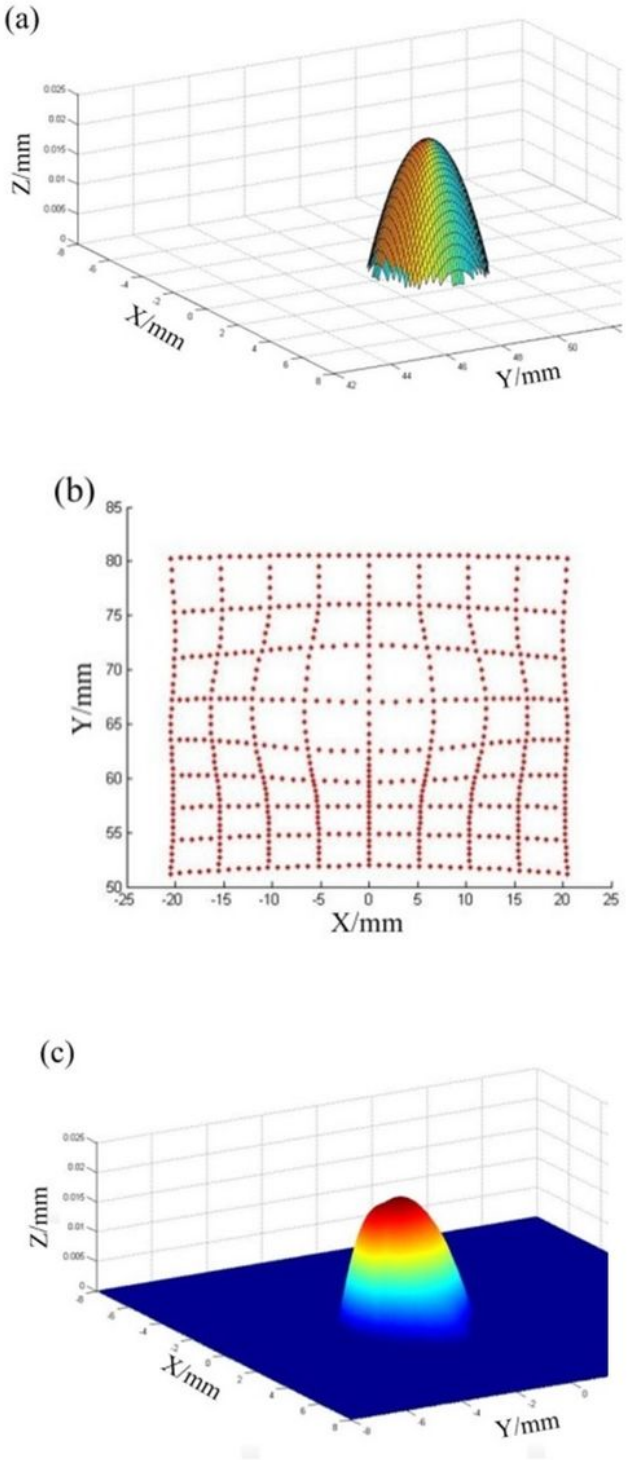

Figure 8

Recovery process of Gaussian convexity (standard Gaussian convexity (projection of the grid laser on the screen (recovered surface

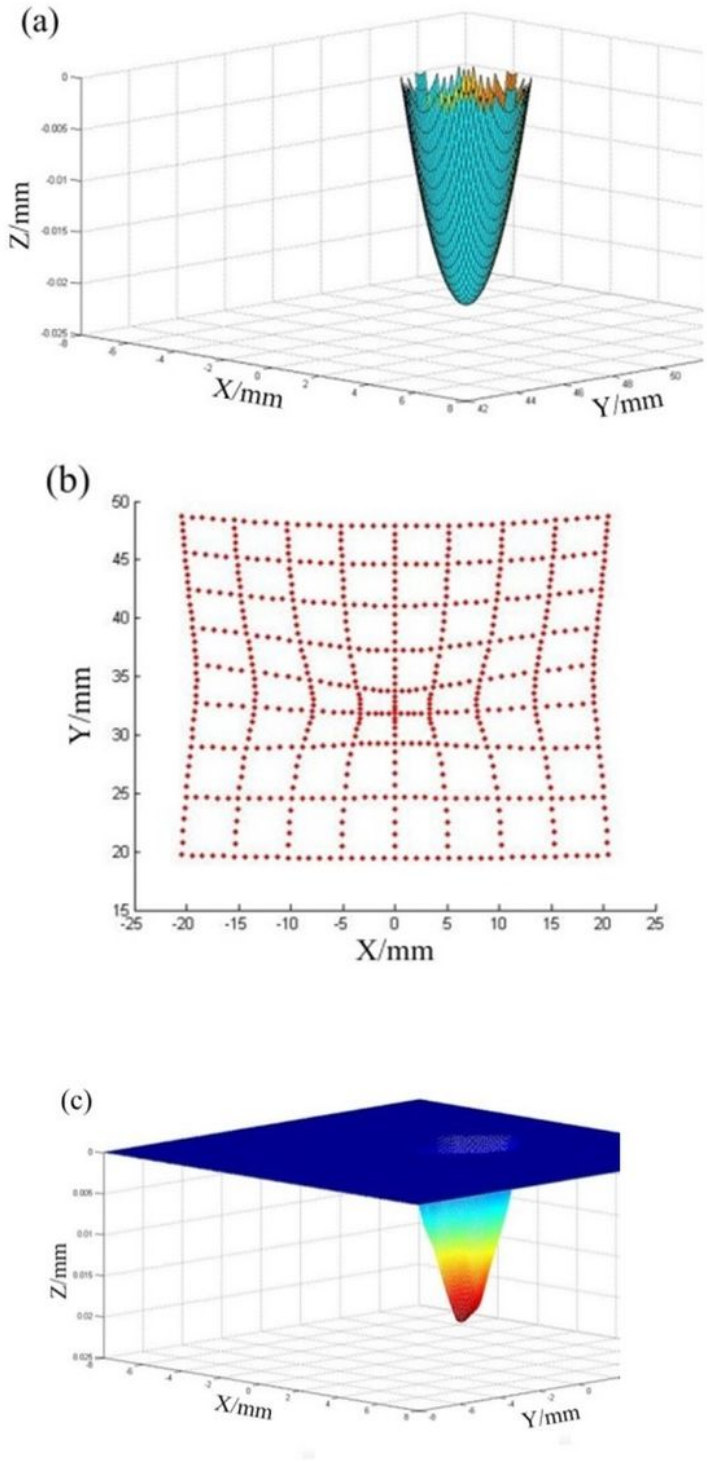

Figure 9

The recovery process of Gaussian concavity: (a) standard Gaussian concavity (b) the project ion of grid laser on the screen (c) the recovered surface

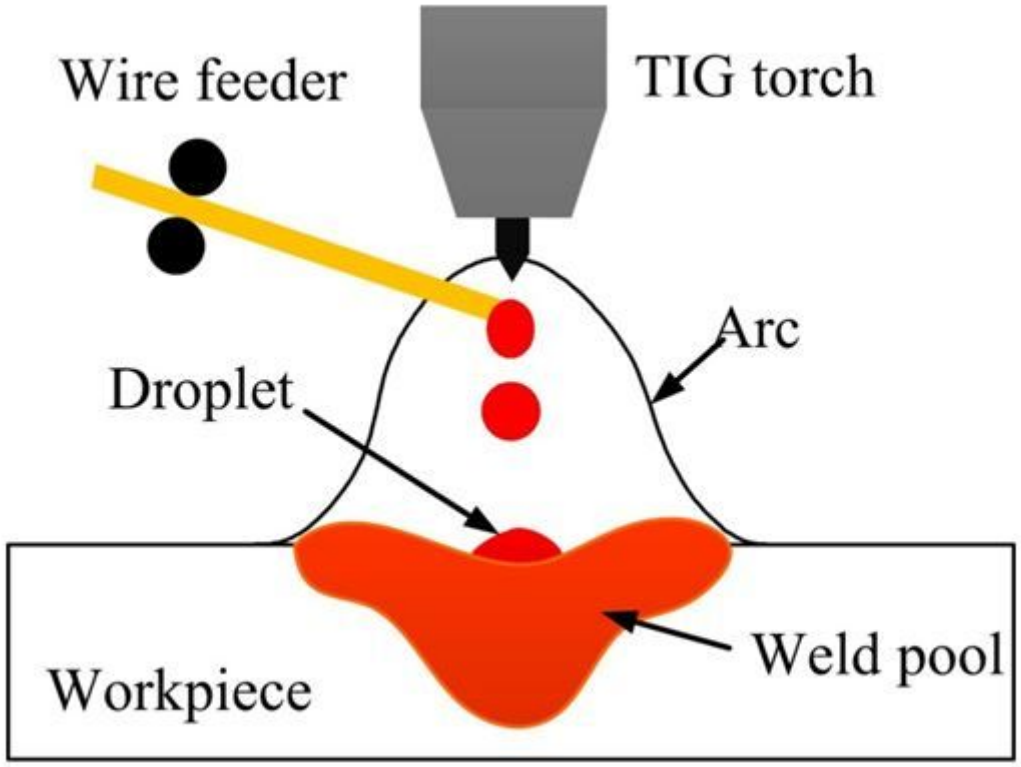

Figure 10

Diagram of the drop transfer model for TIG welding

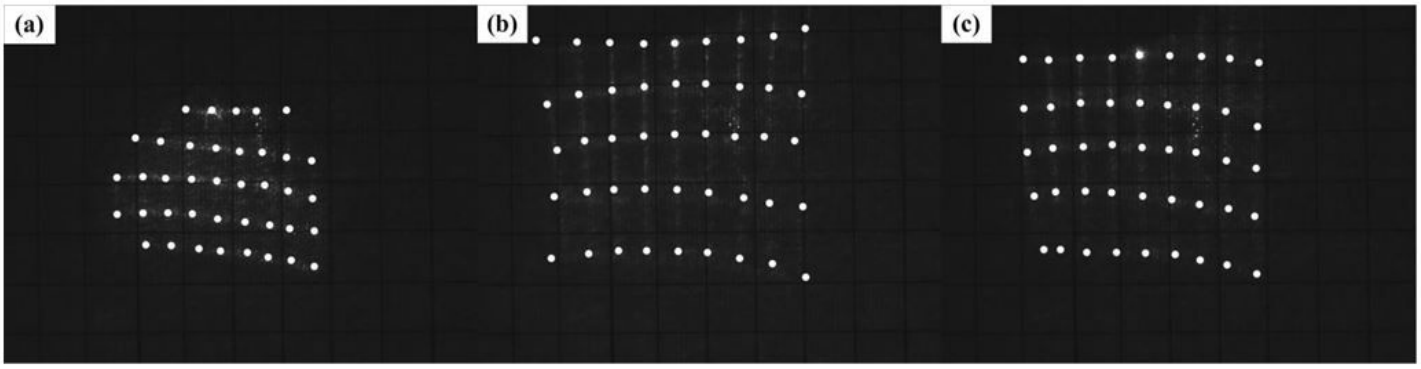

Figure 11

Imaging of the grid laser (T=0 s (T=0 05s , and (T=0.13s

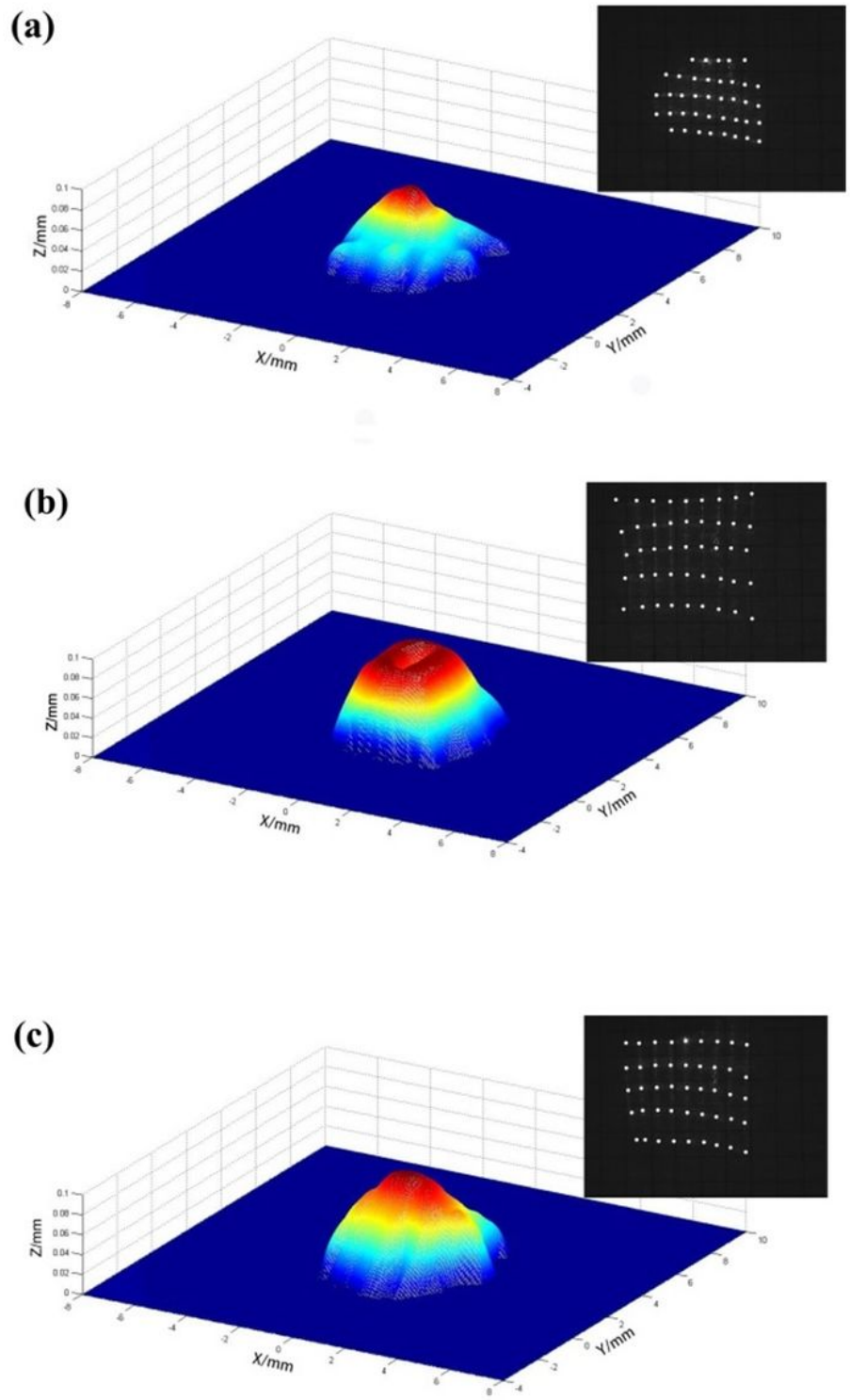

Figure 12

Reconstruction of the droplet dropping process: (a)T=0 s, (b)T=0.05 s, (c)T=0.13 s.

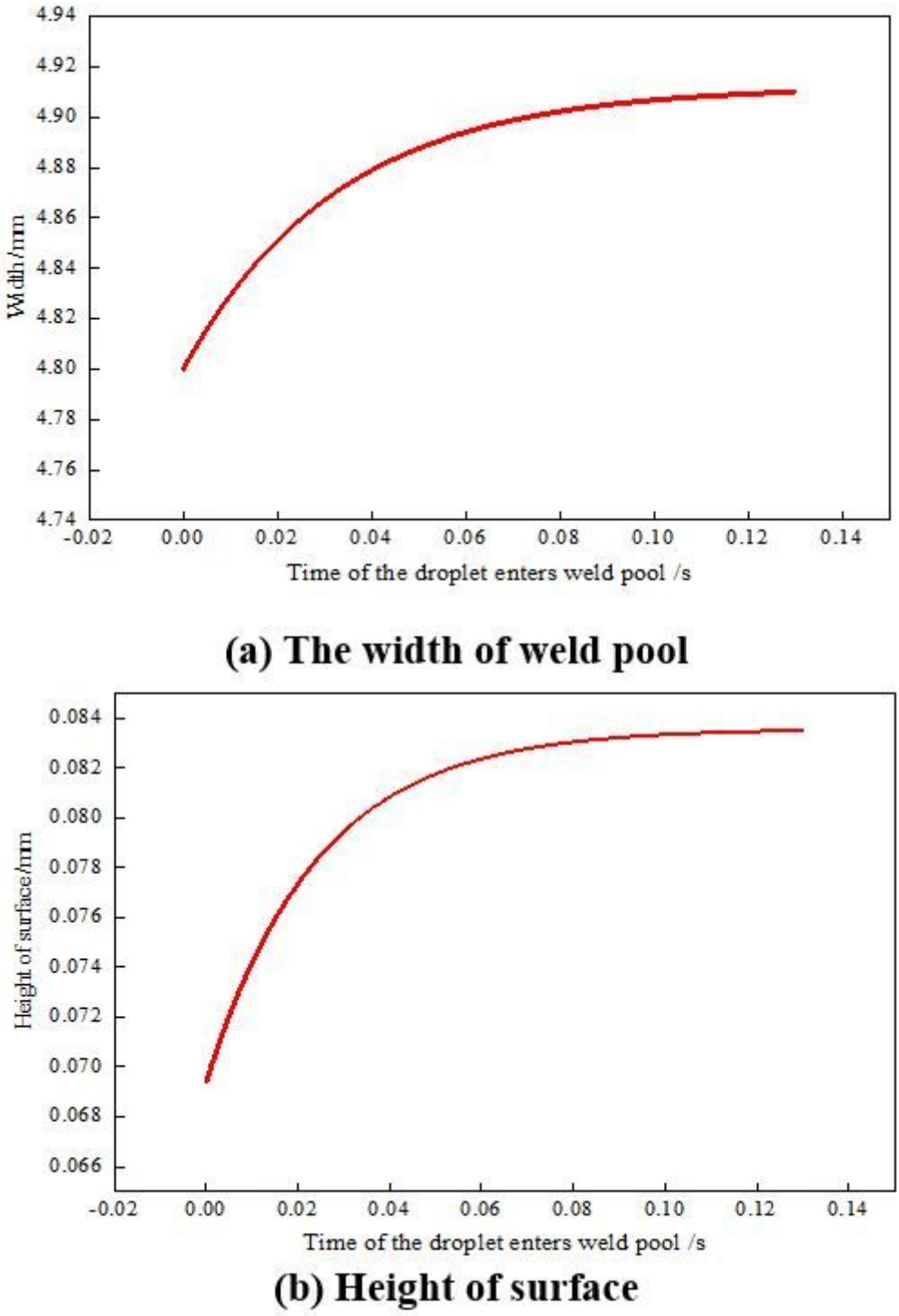

Figure 13

Comparison of experimental results and recovery results.

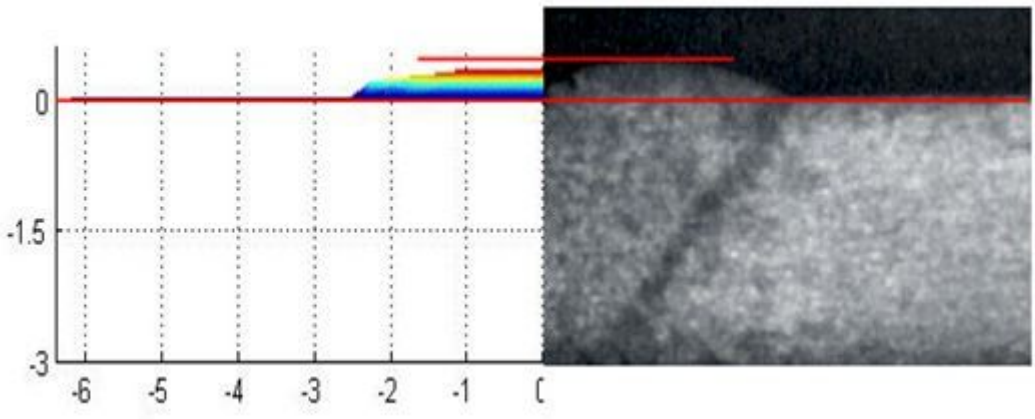

Figure 14

Cross section comparison between test results and recovery results.